THE ASTROPHYSICAL JOURNAL, 613:448–459, 2004 September 20

PROMPT GAMMA-RAY BURST SPECTRA: DETAILED CALCULATIONS AND THE EFFECT OF PAIR PRODUCTION

ASAF PE'ER[1] AND ELI WAXMAN[1]

Received 2003 November 11; accepted 2004 May 31

ABSTRACT

We present detailed calculations of the prompt spectrum of γ-ray bursts (GRBs) predicted within the fireball model framework, in which emission is due to internal shocks in an expanding relativistic wind. Our time-dependent numerical model describes cyclo-synchrotron emission and absorption, inverse and direct Compton scattering, and $e^{\pm}$ pair production and annihilation (including the evolution of high-energy electromagnetic cascades). It allows, in particular, a self-consistent calculation of the energy distribution of $e^{\pm}$ pairs produced by photon annihilation and hence, a calculation of the spectra resulting when the scattering optical depth due to pairs, $\tau_{\pm}$, is high. We show that emission peaks at $\sim$1 MeV for moderate-to-large $\tau_{\pm}$, reaching $\tau_{\pm} \sim 10^2$. In this regime of large compactness we find that (1) a large fraction of shock energy can escape as radiation even for large $\tau_{\pm}$; (2) the spectrum depends only weakly on the magnetic field energy fraction; (3) the spectrum is hard, $\varepsilon^2\, dN/d\varepsilon \propto \varepsilon^{\alpha}$ with $0.5 < \alpha < 1$, between the self-absorption ($\varepsilon_{\rm ssa} = 10^{0.5\pm0.5}$ keV) and peak ($\varepsilon_{\rm peak} = 10^{0.5\pm0.5}$ MeV) photon energy; (4) the spectrum shows a sharp cutoff at $\sim$10 MeV; and (5) thermal Comptonization leads to emission peaking at $\varepsilon_{\rm peak} \gtrsim 30$ MeV and cannot, therefore, account for observed GRB spectra. For small compactness, spectra extend to higher than 10 GeV with flux detectable by *GLAST*, and the spectrum at low energy depends on the magnetic field energy fraction. Comparison of the flux at $\sim$1 GeV and $\sim$100 keV may therefore allow the determination of the magnetic field strength. For both small and large compactness, the spectra depend only weakly on the spectral index of the energy distribution of accelerated electrons.

Subject headings: gamma rays: bursts — gamma rays: theory — methods: data analysis — methods: numerical — radiation mechanisms: nonthermal

Online material: color figures

1. INTRODUCTION

It is widely accepted that γ-ray bursts (GRBs) are produced by the dissipation of kinetic energy in a highly relativistic wind, driven by gravitational collapse of a (few) solar mass object into a neutron star or a black hole (see, e.g., Piran 2000, Mészáros 2002, and Waxman 2003 for reviews). The prompt γ-ray emission is believed to be produced by synchrotron and inverse Compton (IC) emission of electrons accelerated to relativistic energy by internal shocks within the expanding wind (see, however, Lazzati et al. 2000; Ghisellini et al. 2000). Synchrotron emission is favored if the fireball is required to be "radiatively efficient," i.e., if a significant fraction of the fireball energy is required to be converted to γ-rays.

Over a wide range of model parameters, a large number of $e^{\pm}$ pairs are produced in internal collisions, as a result of annihilation of high-energy photons (e.g., Mészáros & Rees 2000; Guetta et al. 2001). In fact, if the internal shocks occur at small enough radii, the plasma becomes optically thick and a second photosphere is formed (Mészáros & Rees 2000; Mészáros et al. 2002) beyond the photosphere associated with the electrons initially present in the fireball. As we show here (§ 2.2; see also Guetta et al. 2001), requiring the emission to be dominated by $\sim$1 MeV photons implies, within the fireball model framework, a moderate-to-large optical depth due to scattering by pairs. When the scattering optical depth due to pairs is high, calculation of the emergent spectrum becomes complicated. Relativistic pairs cool rapidly to mildly relativistic energy, where their energy distribution is determined by a balance between emission and absorption of radiation. The emergent spectrum, which is affected by scattering off the pair population, depends strongly on the pair energy distribution, and in particular on the "effective temperature" that characterizes the low end of the energy distribution. The pair energy distribution is difficult to calculate analytically. Moreover, analytic calculation of the spectrum emerging from the electromagnetic cascades initiated by photon annihilation is also difficult. Therefore, in order to derive the emergent spectrum, a numerical model is needed (see, e.g., Ghisellini & Celotti 1999; Zhang & Mészáros 2002).

Emission from steady plasma, where pair production and annihilation are taken into consideration, was numerically studied in the past in the context of active galactic nuclei (AGNs). It was found that thermal plasma, optically thin to Thomson scattering and characterized by a comoving compactness $10 \lesssim l' \lesssim 10^3$, has a normalized pair temperature $\theta \equiv kT/m_ec^2 \approx 10^{-2}$ to 10^{-1} (Lightman 1982; Svensson 1982b, 1984). The dimensionless compactness parameter l is defined by $l \equiv L\sigma_{\rm T}/Rm_ec^3$, where L is the luminosity and R is a characteristic length of the object. The above result holds also in a scenario considering injection of high-energy particles, which lose their energy via IC scattering of low-energy photons and thermalize before annihilating (Svensson 1987; Lightman & Zdziarski 1987). The optical depth for scattering by pairs was found in the above analyses to be $0.1 \lesssim \tau_{\pm} \lesssim 15$. However, $\tau_{\pm}$ strongly depends on the comoving compactness l' and sharply increases beyond these values when the compactness increases beyond 10^3 (see Lightman & Zdziarski 1987; Svensson 1987). When the scattering optical depth

[1] Physics Faculty, Weizmann Institute, Rehovot 76100, Israel; asaf@wicc.weizmann.ac.il.

$\tau_{\pm} \gg 1$ and $\theta \ll 1$, solving the Kompaneets equation gives a cutoff at normalized photon energy $h\nu/m_e c^2 \simeq 1/\tau_{\pm}^2$ (Sunyaev & Titarchuk 1980).

The results mentioned above are not directly applicable to GRB plasma. The GRB plasma is rapidly evolving, and steady state cannot be assumed. For example, the electron distribution function does not reach thermal equilibrium, even at low energy (see § 4); because of expansion, the average number of scatterings a photon undergoes is $\sim\tau_{\pm}$ rather than $\tau_{\pm}^2$; the expansion (and cooling) of plasma electrons has a significant effect on the photon spectrum when $\tau_{\pm}$ is high. Moreover, significant luminosity at high energies (exceeding the pair production threshold) is expected because of synchrotron emission from energetic particles in strong magnetic fields, $B \sim 10^5$–10^6 G, typical for GRB shell-shell collision phase, a phenomenon that was not considered in the analyses mentioned above. And last, in the GRB case a nonthermal high-energy electron population is assumed to be produced, which leads at large compactness to the formation of a rapid electromagnetic cascade, the evolution of which was not considered in the past.

A numerical calculation of GRB spectra that takes into consideration creation and annihilation of pairs is complicated. The evolution of electromagnetic cascades initiated by the annihilation of high-energy photons occurs on a very short timescale. On the other extreme, evolution of the low-energy, mildly relativistic pairs, which is governed by synchrotron self-absorption, direct Compton emission, and IC emission, takes a much longer time. The large difference in characteristic timescales poses a challenge to numeric calculations. For this reason, the only numerical approach so far (Pilla & Loeb 1998) was based on a Monte Carlo method. This model, however, did not consider the parameter space region where pairs strongly affect the spectra. Another challenge to numerical modeling is that at mildly relativistic energies the usual synchrotron emission and IC scattering approximations are not valid, and precise cyclo-synchrotron emission, direct Compton scattering, and IC scattering calculations are required.

In this work, we consider emission in the fireball model framework, resulting from internal shocks within an expanding relativistic wind. These shock waves dissipate kinetic energy and accelerate a population of relativistic electrons. We adopt the common assumption of a power-law energy distribution of the accelerated particles and calculate the emergent spectra. We present the results of time-dependent numerical calculations, considering all the relevant physical processes: cyclo-synchrotron emission, synchrotron self-absorption, inverse and direct Compton scattering, and $e^{\pm}$ pair production and annihilation, including the evolution of high-energy electromagnetic cascades. A full description of the numerical code will appear in A. Pe'er & E. Waxman (2004, in preparation).

We note that Comptonization by a thermal population of electrons (and possibly $e^{\pm}$ pairs) was considered as a possible mechanism for GRB production (e.g., Ghisellini & Celotti 1999), following the evidence that, at least in some cases, the GRB spectra at low energy are steeper at early times than expected for synchrotron emission (Crider et al. 1997; Preece et al. 2002; Frontera et al. 2000). This model is different from the common model considered in the previous paragraph in assuming both that the kinetic energy dissipated in a collision between two "shells" within the expanding wind is continuously distributed among all shell electrons, rather than being deposited at any given time into a small fraction of shell electrons that pass through the shock wave, and also that energy is equally distributed among electrons, rather than following a power-law distribution. There is no known acceleration mechanism that leads to the above energy distribution among electrons, and the spectrum predicted in this scenario does not account for the claimed steep spectra, which may be naturally explained as a contribution to the observed γ-ray radiation of photospheric fireball emission (e.g., Mészáros & Rees 2000). It is nevertheless worthwhile to derive the spectrum that is expected from thermal Comptonization under plasma conditions typical to GRB fireballs. This will allow the determination of whether this process may significantly contribute to GRB γ-ray emission. Our numerical code enables an accurate calculation of the pair temperature in this scenario, as well as a reliable calculation of the emergent spectrum.

This paper is organized as follows. In § 2.1 we derive the plasma parameters at the internal shock stage and their dependence on uncertain model parameter values. In § 2.2 it is shown that moderate-to-large compactness is expected for the parameter range in which emission peaks at $\sim$1 MeV, and approximate analytic results describing the emission in this regime are given. Our numerical methods are briefly presented in § 3; a detailed description of the model will be found in A. Pe'er & E. Waxman (2004, in preparation). Our numerical results for the scenario of acceleration of particles in shock waves are presented in § 4. In § 5 we present both analytical and numeric calculations of the spectra resulting from thermal Comptonization. We summarize and conclude our discussion in § 6, with special emphasis on observational implications.

2. PLASMA PARAMETERS AND LARGE COMPACTNESS BEHAVIOR

Variability in the Lorentz factor of the relativistic wind emitted by the GRB progenitor leads to the formation of shock waves within the expanding wind at radii larger than the underlying source size. If we denote with Γ the characteristic wind Lorentz factor and assume variations $\Delta\Gamma/\Gamma \sim 1$ on timescale Δt, shocks develop at radius $r_i \approx 2\Gamma^2 c\Delta t = 5.4 \times 10^{11}\Gamma_{2.5}^2 \Delta t_{-4}$ cm. For $\Delta\Gamma/\Gamma \sim 1$ the shocks are mildly relativistic in the wind frame. For our calculations, we consider a collision between two uniform shells of thickness $c\Delta t$, in which two mildly relativistic ($\Gamma_s - 1 \sim 1$ in the wind frame) shocks are formed, one propagating forward into the slower shell ahead, and one propagating backward (in the wind frame) into the faster shell behind. The comoving shell width, measured in the shell rest frame, is $\Delta R = \Gamma c\Delta t$, and the comoving dynamical time, the characteristic time for shock crossing and shell expansion measured in the shell rest frame, is $t_{\rm dyn} = \Gamma\Delta t$.

Under these assumptions, the shocked plasma conditions are determined by six model parameters. Three are related to the underlying source: the total luminosity $L = 10^{52}L_{52}$ ergs s^{-1}, the Lorentz factor of the shocked plasma $\Gamma = 10^{2.5}\Gamma_{2.5}$, and the variability time $\Delta t = 10^{-4}\Delta t_{-4}$ s. Three additional parameters are related to the collisionless-shock microphysics: the fraction of postshock thermal energy carried by electrons $\epsilon_e = 10^{-0.5}\epsilon_{e,-0.5}$, that carried by magnetic field $\epsilon_B = 10^{-0.5}\epsilon_{B,-0.5}$, and the power-law index of the accelerated electrons energy distribution $d\log n_e/d\log\varepsilon_e = -p$. In the following calculations spherical geometry is assumed. However, the results are valid also for a jetlike GRB, provided that the jet opening angle $\theta > \Gamma^{-1}$ (in which case L should be regarded as the isotropic equivalent luminosity).

In § 2.1 we derive the characteristic values of plasma parameters obtained under the adopted model assumptions, as well as the characteristic synchrotron and self-absorption frequencies. Since, as we show in § 2.2, the compactness parameter is related to the optical depths for both pair production and scattering by pairs, emission from plasma characterized by small compactness is well approximated by the optically thin synchrotron self-Compton emission model. This model, however, ceases to be valid for large values of the compactness. In § 2.2 we give an approximate analysis of the emission of radiation from plasma of moderate-to-large compactness.

2.1. *Plasma Parameters*

With θ_p denoting the average proton internal energy (associated with random motion) in the shocked plasma, measured in units of the proton's rest mass, the comoving proton density in the shocked plasma is given by

$$n_p \approx \frac{L}{4\pi r_i^2 c\Gamma^2 \theta_p m_p c^2} = 6.7\times 10^{14} L_{52}\Gamma_{2.5}^{-6}\Delta t_{-4}^{-2}\theta_p^{-1}\ \mathrm{cm}^{-3}. \quad (1)$$

For mildly relativistic shocks, $\theta_p \sim 1$ and is limited within the fireball model framework to $\theta_p \lesssim$ a few, since the Lorentz factors of the internal shocks cannot be larger than a few. This is due to the fact that the Lorentz factors of colliding shells cannot differ by significantly more than an order of magnitude: shells' Lorentz factors are limited to the range of $\sim$100 to a few thousand, where the lower limit of $\sim$100 is set by the requirement to avoid too large an optical depth, and the upper limit of few times 10^3 is due to the fact that shells cannot be accelerated by the radiation pressure to Lorentz factors $\gg 10^3$ (e.g., § 2.3 in Waxman 2003).

A fraction ϵ_B of the internal energy density $u_{\rm int} = L/(4\pi r_i^2 c\Gamma^2)$ is assumed to be carried by the magnetic field, implying that

$$B = \sqrt{\frac{\epsilon_B L}{2\Gamma^6 c^3 \Delta t^2}} = 2.9\times 10^6 L_{52}^{1/2}\epsilon_{B,-0.5}^{1/2}\Gamma_{2.5}^{-3}\Delta t_{-4}^{-1}\ \mathrm{G}. \quad (2)$$

Equating the particle acceleration time, $t_{\rm acc} \simeq \varepsilon/(cqB)$, and the synchrotron cooling time, $t_{\rm cool,\,sync}$, gives the maximum Lorentz factor of the accelerated electrons, $\gamma_{\max} = (3/2)m_e c^2 (q^3 B)^{-1/2} = 6.9\times 10^4 L_{52}^{-1/4}\epsilon_{B,-0.5}^{-1/4}\Gamma_{2.5}^{3/2}\Delta t_{-4}^{1/2}$, and the maximum observed energy of the synchrotron-emitted photons,

$$\varepsilon_{\max}^{\rm ob} = \hbar\frac{3}{2}\frac{qB}{m_e c}\gamma_{\max}^2\frac{\Gamma}{1+z} = 7\times 10^{10}(1+z)^{-1}\Gamma_{2.5}\ \mathrm{eV}. \quad (3)$$

The minimum Lorentz factor of the power law–accelerated electrons, given by

$$\gamma_{\min} = \begin{cases} \epsilon_e\theta_p\left(\dfrac{m_p}{m_e}\right)\log^{-1}\left(\dfrac{\varepsilon_{e,\max}}{\varepsilon_{e,\min}}\right), & p=2, \\ \epsilon_e\theta_p\left(\dfrac{m_p}{m_e}\right)\dfrac{p-2}{p-1}, & p>2, \end{cases} \quad (4)$$

is much larger than γ_c, the Lorentz factor of electrons that cool on a timescale equal to the dynamical timescale, which is $\gamma_c \sim 1$.

For a typical value of $\log(\varepsilon_{e,\max}/\varepsilon_{e,\min}) \simeq 7$, synchrotron emission from the least energetic electrons peaks at

$$\varepsilon_{\rm peak}^{\rm ob} = \begin{cases} 10^5(1+z)^{-1}L_{52}^{1/2}\epsilon_{e,-0.5}^2\epsilon_{B,-0.5}^{1/2}\Gamma_{2.5}^{-2}\Delta t_{-4}^{-1}\theta_p^2\ \mathrm{eV}, & p=2, \\ 5.5\times 10^6\left(\dfrac{p-2}{p-1}\right)^2(1+z)^{-1} & \\ \quad\times L_{52}^{1/2}\epsilon_{e,-0.5}^2\epsilon_{B,-0.5}^{1/2}\Gamma_{2.5}^{-2}\Delta t_{-4}^{-1}\theta_p^2\ \mathrm{eV}, & p>2. \end{cases} \quad (5)$$

The self-absorption optical depth $\tau_\nu = \alpha_\nu\Gamma c\Delta t$, calculated using the absorption coefficient

$$\alpha_\nu = \begin{cases} 1.3\times 10^{41}\nu^{-3}L_{52}^2\Gamma_{2.5}^{-12}\epsilon_{e,-0.5}\epsilon_{B,-0.5}\Delta t_{-4}^{-4}\ \mathrm{cm}^{-1}, & p=2, \\ 1.3\times 10^{51}\nu^{-7/2}L_{52}^{9/4}\Gamma_{2.5}^{-27/2} & \\ \quad\times\epsilon_{e,-0.5}^2\epsilon_{B,-0.5}^{5/4}\Delta t_{-4}^{-9/2}\ \mathrm{cm}^{-1}, & p=3 \end{cases} \quad (6)$$

(Rybicki & Lightman 1979), is less than 1 at $\varepsilon_{\rm peak}$,

$$\tau_{\rm ssa,\,peak} = \begin{cases} 0.23L_{52}^{1/2}\epsilon_{e,-0.5}^{-5}\epsilon_{B,-0.5}^{-1/2}\Gamma_{2.5}^{-2}\theta_p^{-6}, & p=2, \\ 8.5\times 10^{-4}L_{52}^{1/2}\epsilon_{e,-0.5}^{-5}\epsilon_{B,-0.5}^{-1/2}\Gamma_{2.5}^{-2}\theta_p^{-7}, & p=3. \end{cases} \quad (7)$$

If the fraction of thermal energy carried by the magnetic field is very small, $\epsilon_B \leq 10^{-5}L_{52}^{-1}\Gamma_{2.5}^5\Delta t_{-4}\epsilon_{e,0.5}^{-1}$, the electrons are in the slow cooling regime (i.e., $\gamma_{\min} < \gamma_c$), the power radiated per unit energy below $\varepsilon_{\rm peak}$ is proportional to $(\varepsilon/\varepsilon_{\rm peak})^{1/3}$, and the energy below which the optical depth becomes greater than 1, $\varepsilon_{\rm ssa} = \varepsilon_{\rm peak}\tau_{\rm ssa,\,peak}^{3/5}$, is

$$\varepsilon_{\rm ssa}^{\rm ob} = \begin{cases} 5\times 10^3(1+z)^{-1}L_{52}^{4/5}\epsilon_{e,-0.5}^{-1}\epsilon_{B,-5}^{1/5} & \\ \quad\times\Gamma_{2.5}^{-16/5}\Delta t_{-4}^{-1}\theta_p^{-8/5}\ \mathrm{eV}, & p=2, \\ 2.5\times 10^3(1+z)^{-1}L_{52}^{4/5}\epsilon_{e,-0.5}^{-1}\epsilon_{B,-5}^{1/5} & \\ \quad\times\Gamma_{2.5}^{-16/5}\Delta t_{-4}^{-1}\theta_p^{-11/5}\ \mathrm{eV}, & p=3. \end{cases} \quad (8)$$

When cooling is important ($\gamma_{\min} > \gamma_c$), as is the case for typical fireball parameters, the electron energy distribution, and hence the self-absorption frequency, are modified. As we show below (§ 4), for large compactness the energy distribution of electrons and pairs is quasi-Maxwellian. For a thermal distribution of electrons and positrons, with normalized temperature $\theta \equiv kT/m_e c^2$ and normalized pair density $f \equiv n_\pm/n_p$, the self-absorption frequency ν_t is approximated by (using the results of Mahadevan et al. 1996 for cyclo-synchrotron emission)

$$\nu_t = 5\times 10^{14}L_{52}^{0.6}\epsilon_{B,-0.5}^{0.45}\Gamma_{2.5}^{-10/3}\Delta t_{-4}^{-1}\theta_{-1}f_1^{1/6}\ \mathrm{Hz}, \quad (9)$$

where $\theta = 0.1\theta_{-1}$ and $f = 10f_1$. This result is accurate to better than 10% for parameters in the ranges $0.001 < L_{52} < 10$, $0.01 < \epsilon_B \leq 0.33$, $100 < \Gamma < 1000$, $0.1 < \theta < 5$, and $1 \leq f < 100$. The values of θ and f were found numerically (§ 4) to be within these limits for a wide range of parameters that characterize GRBs. Therefore,

$$\begin{aligned}\epsilon_{\rm ssa,thermal}^{\rm ob} &= h\nu_t\Gamma(1+z)^{-1} \\ &\approx 600(1+z)^{-1}L_{52}^{0.6}\epsilon_{B,-0.5}^{0.45}\Gamma_{2.5}^{-7/3}\Delta t_{-4}^{-1}\theta_{-1}f_1^{1/6}\ \mathrm{eV}.\end{aligned} \quad (10)$$

2.2. *Large-Compactness Behavior*

The comoving compactness parameter l' is defined as $l' = \Delta R n'_\gamma \sigma_T$, where $\Delta R = ct_{\rm dyn}$ is the comoving width and $n'_\gamma = \epsilon_e L/(4\pi m_e c^3 \Gamma^2 r_i^2)$ is the comoving number density of photons with energy exceeding the electron's rest mass, $\varepsilon_{\rm ph} \geq m_e c^2$ (in the plasma rest frame). Only these photons are of interest, as their number density determines the number density of the produced pairs. In deriving the last equation, a mean photon energy (in the comoving frame) of $\langle \varepsilon_{\rm ph} \rangle \approx m_e c^2$ is assumed. This assumption is valid as long as the spectral index α ($\varepsilon^2 dN/d\varepsilon \propto \varepsilon^\alpha$) is not significantly different from 0, and it leads to

$$l' = \frac{\epsilon_e L \sigma_T}{16\pi m_e c^4 \Gamma^5 \Delta t} = 250 L_{52} \epsilon_{e,-0.5} \Gamma_{2.5}^{-5} \Delta t_{-4}^{-1}$$
$$= 520 \left(\frac{1+z}{2} \varepsilon^{\rm ob}_{\rm peak,1\ MeV} \right)^2 \Delta t_{-2} \Gamma_{2.5}^{-1} \epsilon_{e,-0.5}^{-3} \epsilon_{B,-0.5}^{-1} \theta_{p,0.5}^{-4}. \quad (11)$$

Here $\theta_p = 10^{0.5}\theta_{p,0.5}$ and $\Delta t = 10^{-2}\Delta t_{-2}$ s. Equation (11) also implies, using equation (5), that

$$\varepsilon^{\rm ob}_{\rm peak} = 0.3 \frac{2}{1+z} l_2'^{2/5} L_{52}^{1/10} \Delta t_{-2}^{-3/5} \epsilon_{e,-0.5}^{8/5} \epsilon_{B,-0.5}^{1/2} \theta_{p,0.5}^2 \text{ MeV}, \quad (12)$$

where $l' = 10^2 l'_2$. Equation (12) implies that emission peaking at $\sim$1 MeV may be obtained with small compactness, $l' \sim 1$, only for very short variability time, $\Delta t \leq 10^{-4.5}$ s, and, using equation (11), large Γ, $\Gamma \geq 10^3$. For the longer variability time commonly assumed in modeling GRBs ($\Delta t \sim 1$–10 ms; e.g., Piran 2000; Mészáros 2002; Waxman 2003), $l' \gg 1$ is obtained for the parameter range in which synchrotron emission peaks at $\sim$1 MeV. The main goal of the present analysis is to examine the modification of the spectrum due to the formation of pairs in GRB plasma of moderate-to-large compactness.

The following point should be noted here. The variability time Δt in the range of $\sim$1–10 ms is commonly adopted, since $\sim$1 ms variability has been observed in some bursts (Bhat et al. 1992; Fishman et al. 1994), and most bursts show variability on a $\sim$10 ms timescale (Woods & Loeb 1995; Walker et al. 2000). It should be kept in mind, however, that variability on much shorter timescales would not have been possible to resolve experimentally and cannot therefore be ruled out.

Large l' implies large optical depth to photon-photon pair production, $\tau_{\gamma\gamma} \approx l' > 1$, and also large optical depth to Thomson scattering by pairs, $\tau_\pm$. In the absence of pair annihilation, $\tau_\pm \approx 2l'$. For $l' \gg 1$, $\tau_\pm$ is expected to be large, implying also that pair annihilation is important, since the cross section for pair annihilation is similar to σ_T [$v\sigma_\pm(v) \sim c\sigma_T$ for subrelativistic relative velocity v]. The optical depth $\tau_\pm$ may be estimated in this case as follows. As we show in § 4, photons and pairs approach in the case of $l' \gg 1$ a quasi-thermal distribution with mildly relativistic effective temperature (or characteristic energy), $\theta m_e c^2$ with $\theta \ll 1$. Under these conditions, the production of pairs via photon annihilation, which for $l' \gg 1$ occurs on a timescale much shorter than the dynamical time and may therefore be approximated as the rate of energy production (per unit volume) in more than $m_e c^2$ photons, $\sim\left(\epsilon_e L/4\pi r_i^2 \Gamma^2 c\right)/\left(m_e c^2 t_{\rm dyn}\right)$, is balanced by pair annihilation, the rate of which is given by $\sim n_\pm^2 c\sigma_T$. This implies that $n_\pm \sim l'^{1/2}/\sigma_T c t_{\rm dyn}$ and

$$\tau_\pm \approx l'^{1/2}. \quad (13)$$

If synchrotron photons (of energy lower than the pair production threshold $\sim m_e c^2$) and pairs reach a quasi-thermal distribution via Compton and IC scattering interactions, then the pair "effective temperature" may be estimated as follows. The energy of low-energy photons is increased over a dynamical time by a factor $\simeq \exp(4\tau_\pm \theta)$ (note that, as a result of plasma expansion, the number of scatterings is $\tau_\pm$, rather than $\tau_\pm^2$). The energy ε_0 of the lowest energy photons that reach "thermalization" is therefore given by $\varepsilon_0 \exp(4\tau_\pm\theta) \approx \theta m_e c^2$. Assuming that $\varepsilon_0 > \varepsilon_{\rm peak}$ and that the synchrotron spectrum is flat, $\varepsilon^2 dN/d\varepsilon \propto \varepsilon^0$, the average energy per photon for synchrotron photons in the energy range $\varepsilon_0 < \varepsilon < m_e c^2$ is $\simeq \varepsilon_0 \log(m_e c^2/\varepsilon_0)$. Since the number of photons is conserved in Compton scattering interactions, and since the number of pairs is much smaller than the number of photons ($\tau_\pm \approx l'^{1/2}$), conservation of energy implies that $\varepsilon_0 \log(m_e c^2/\varepsilon_0) \simeq \theta m_e c^2$. Using the relation $\varepsilon_0 \exp(4\tau_\pm\theta) \approx \theta m_e c^2$, we therefore find $4\theta\tau_\pm \approx \log[4\theta\tau_\pm - \log(\theta)]$, which implies $4\theta\tau_\pm \sim 2$ over a wide range of values of $\tau_\pm \gg 1$. The observed effective temperature, $\Gamma\theta$, is therefore

$$(1+z)^{-1}\Gamma\theta m_e c^2 \approx (1+z)^{-1} \frac{\Gamma}{2(l')^{1/2}} m_e c^2$$
$$= 5 \frac{2}{1+z} \left(\frac{L_{52}\epsilon_{e,-0.5}}{\Delta t_{-4}} \right)^{1/5} \left(l'_2\right)^{-7/10} \text{ MeV}. \quad (14)$$

For large optical depth, $\tau_\pm \gg 1$, the plasma expands before photons escape. Assuming that the electrons and photons cool "adiabatically," i.e., that the characteristic energy of escaping photons $\theta \propto V^{-1/3}$, where V is the specific volume, is lower than given by equation (14) by a factor of $\tau_\pm^{-1/2}$ (since the optical depth falls off as $V^{-2/3}$). The observed characteristic photon energy is therefore

$$\varepsilon^{\rm ob} \approx (1+z)^{-1} \frac{\Gamma\theta m_e c^2}{\tau_\pm^{1/2}} \approx (1+z)^{-1} \frac{\Gamma}{2(l')^{3/4}} m_e c^2$$
$$= 2 \frac{2}{1+z} \left(\frac{L_{52}\epsilon_{e,-0.5}}{\Delta t_{-4}} \right)^{1/5} \left(l'_2\right)^{-19/20} \text{ MeV}. \quad (15)$$

In the limit of $l' \to \infty$ we expect the plasma to reach thermal equilibrium. Assuming that the fraction of dissipated kinetic energy carried by electrons is converted to thermal radiation, the resulting (blueshifted) radiation temperature is

$$\Gamma T = 0.1(1+z)^{-1} l_2'^{1/10} L_{52}^{3/20} \Delta t_{-4}^{-2/5} \epsilon_{e,-0.5}^{-1/10} \text{ MeV}. \quad (16)$$

3. NUMERICAL CALCULATIONS

3.1. *Method*

The acceleration of particles in the internal shock waves is accompanied by time-dependent radiative processes, which are coupled to each other. In order to follow the emergent spectra we developed a time-dependent model, solving the kinetic equations describing cyclo-synchrotron emission, synchrotron self-absorption, Compton scattering ($e\gamma \to e\gamma$), and pair production ($e^+e^- \to \gamma\gamma$) and annihilation ($\gamma\gamma \to e^+e^-$). Our model follows the above-mentioned phenomena over a wide range of energy scales, including the evolution of the rapid electromagnetic cascade at high energies.

The calculations are carried out in the comoving frame, assuming homogeneous and isotropic distributions of both particles and photons in this frame. Relativistic electrons are continuously injected into the plasma at a constant rate and with a predetermined constant power-law index p between $\gamma_{\rm min}$ and $\gamma_{\rm max}$ (see eq. [4]) throughout the dynamical time, during which the shock waves cross the colliding shells. Above $\gamma_{\rm max}$, an exponential cutoff is assumed. The magnetic field is assumed to be time-independent, given by equation (2).

The particle distributions are discretized, spanning a total of 10 decades of energy ($\gamma\beta_{\rm min} = 10^{-3}$ to $\gamma\beta_{\rm max} = 10^{7}$). The photon bins span 14 decades of energy, from $x_{\rm min} \equiv \varepsilon_{\rm min}/m_e c^2 = 10^{-8}$ to $x_{\rm max} \equiv \varepsilon_{\rm max}/m_e c^2 = 10^{6}$. A fixed time step is chosen, typically $10^{-4.5}$ times the dynamical time. Numerical integration, using a Cranck-Nickolson second-order scheme for synchrotron self-absorption and first-order integration scheme for the other processes, is carried out with this fixed time step. At each time step we calculate (1) the energy-loss time of electrons and positrons at various energies (via cyclo-synchrotron emission and IC scattering, taking into account the fact that low-energy electrons can gain energy via direct Compton scattering); (2) the annihilation time of electrons and positrons; and (3) the annihilation and energy-loss time of photons. Electrons, positrons, and photons for which the energy-loss time or annihilation time is smaller than the fixed time step are assumed to lose all their energy in a single time step, producing secondaries that are treated as a source of lower energy particles. The calculation is repeated with shorter time steps, until convergence is reached.

In the calculations, the exact cross sections for each physical phenomenon, valid at all energy ranges, are being used. Calculations of the reaction rate and emergent photon spectrum from Compton scattering follow the exact treatment of Jones (1968). Pair production rate and the spectrum of the emergent pairs are calculated using the results of Bötcher & Schlickeiser (1997). Pair annihilation calculations are carried out using the exact cross section first derived by Svensson (1982a). The power emitted by an electron with an arbitrary Lorentz factor γ in a magnetic field is calculated using the cyclo-synchrotron emission pattern (see Bekefi 1966; Ginzburg & Syrovatskii 1969; Mahadevan et al. 1996).

A full description of the physical processes, the kinetic equations solved, and the numerical methods used will appear in A. Pe'er & E. Waxman (2004, in preparation).

3.2. *Adiabatic Expansion*

Once the two shocks cross the colliding shells, the dissipation of kinetic energy ceases, and the compressed shells expand and cool. The thermal energy carried by protons, electrons (positrons), and the magnetic field decreases and is converted back into kinetic energy. If the scattering optical depth at the end of the dynamical time is small, photons escape the shells and the energy they carry is "lost" from the plasma. If the optical depth is large, then photons interact with the expanding electrons and positrons, and this interaction affects the emerging spectrum. Since the plasma is collisionless and particles are coupled through macroscopic electromagnetic waves, the details of the conversion of thermal to kinetic energy are unknown. For relativistic plasma at thermal equilibrium undergoing adiabatic expansion, the pressure is inversely proportional to $V^{4/3}$, where V is the volume. We assume that the plasma expands in the comoving frame with velocity comparable to the adiabatic sound speed, $c/\sqrt{3}$, that $B \propto V^{-2/3} \propto t^{-2}$, and that electrons and positrons lose energy because of expansion at a rate $d\varepsilon/\varepsilon = -dV/3V$.

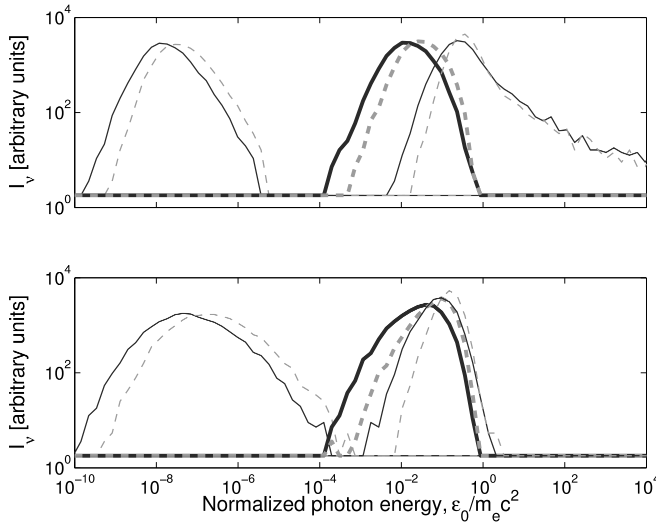

FIG. 1.—Monte Carlo calculations of photon spectra emerging following the injection of monoenergetic photons at the center of an adiabatically expanding sphere of electrons with initial temperature $\theta \equiv kT/m_e c^2 = 0.1$ (see § 3.2). *Top*: Initial scattering optical depth $\tau = 10$; *bottom*: $\tau = 25$. Results are shown for several initial photon energies (normalized to $m_e c^2$): $\varepsilon_0 = 10^{-8}$ (*left*, *thin lines*), $\varepsilon_0 = 10^{-2}$ (*middle*, *thick lines*), and $\varepsilon_0 = 10^4$ (*right*, *thin lines*). Solid lines show the results of complete calculations, while dashed lines show results of calculations in which energy loss of photons due to the bulk motion of electrons is neglected. [*See the electronic edition of the Journal for a color version of this figure.*]

Since our numerical model is spatially "zero-dimensional," we calculate the evolution of the photon and particle spectrum in the scenario outlined in the previous paragraph, assuming a uniform isotropic particle and photon distribution. This calculation does not take into account the energy loss of photons due to the bulk expansion velocity of the electrons, which implies that photons are more likely to collide with electrons that move away from (rather than toward) them. In order to estimate the effect of this energy loss, we have carried out the following calculations.

We have calculated, using a Monte Carlo technique, the evolution of the momentum of a monoenergetic beam of photons emitted at the center of an expanding spherical ball of thermal electron plasma until they escape. The plasma ball was assumed to expand with radial velocity $v(r) = [r/R(t)]c/\sqrt{3}$, where $R(t)$ is the ball radius, and its temperature was assumed to decrease as $\theta \propto R^{-1}$ from an initial value of $\theta = 0.1$. The emergent photon spectrum is shown in Figure 1 for three different initial photon energies, $\varepsilon_0/m_e c^2 = 10^{-8}$, 10^{-2}, and 10^4, and two initial scattering optical depths, $\tau = 10$ and 25. We repeated these calculations, omitting the energy loss of the photons due to the bulk motion of the electrons, by assuming $v = 0$ (while keeping the ball expansion and temperature decrease unchanged). Figure 2 shows the ratio of the average energy of emerging photos with and without inclusion of energy loss to bulk motion for several initial optical depths, as a function of the initial photon energy. This figure demonstrates that the effect of energy loss to bulk expansion is not highly dependent on the initial photon energy and that it leads to reduction of photon energy by a factor of $\sim$3 for initial optical depths in the range of 10–100.

In the numerical calculations presented in §§ 4 and 5 we have corrected for the effect of energy loss due to bulk motion

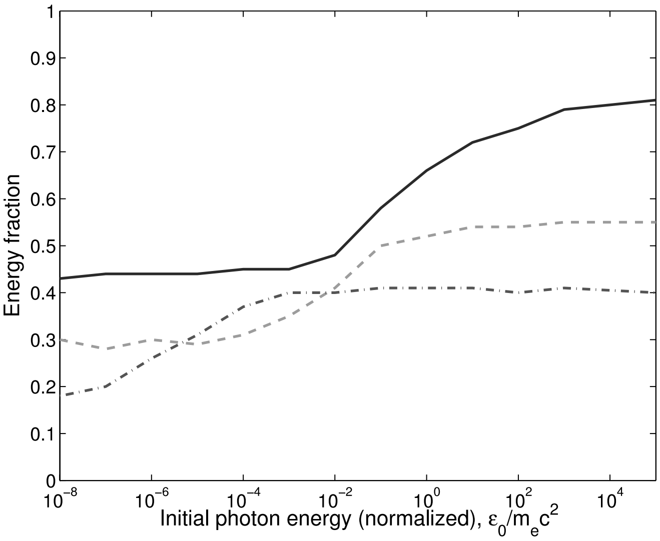

FIG. 2.—Ratio of the average energy of photons emerging from an expanding sphere (see Fig. 1) with and without inclusion of energy loss to bulk motion. Results shown for several initial optical depths: $\tau = 10$ (*solid line*), 25 (*dashed line*), and 100 (*dash-dotted line*). [*See the electronic edition of the Journal for a color version of this figure.*]

by multiplying the emerging photon energy by the (energy-dependent) factor inferred from the calculations presented in Figure 2. This correction is applied for photons of energy exceeding the self-absorption energy $\varepsilon_{\rm ssa}$ at the beginning of the expansion phase. For photons of energy lower than the self-absorption energy $\tilde{\varepsilon}_{\rm ssa}$ at the end of the expansion phase, where the optical depth drops to unity, we have applied no correction. This is due to the fact that photons at these energies are tightly coupled to the electrons, that they are continuously emitted and absorbed, and that this coupling is the dominant factor determining the photons' energy. Note that the self-absorption energy decreases during the adiabatic expansion as the density and the magnetic field decrease. At the intermediate energy range, $\varepsilon_{\rm ssa}$ to $\tilde{\varepsilon}_{\rm ssa}$, we have applied an interpolated correction factor.

Figure 3 presents an example of the modification of the spectrum due to bulk expansion. Since the fractional energy loss is not strongly energy dependent, the correction we apply does not lead to significant distortion of the spectrum. Note, however, that since we do not take into account the spread in the energy of emerging photons that initially had the same energy (see Fig. 1), but rather apply a single correction factor appropriate for the average energy of emerging photons, the emerging spectrum would in reality be somewhat "smeared" compared to our calculation. In particular, the annihilation peak that appears at $\sim$100 MeV is expected to be "smoothed."

4. RESULTS

We have shown in § 2.2 that $l' \gg 1$ is obtained for the parameter range in which synchrotron emission in the fireball model peaks at $\sim$1 MeV (see eq. [12]). In this section we present detailed numerical calculations investigating the emission of radiation at moderate-to-large compactness (for completeness, we present in § 4.1 numerical results also for low compactness). We have demonstrated in § 2.2 that for large compactness the characteristics of emitted radiation are determined mainly by l', with weak dependence on the values of other parameters (see, e.g., eq. [15]). The results presented in §§ 4.3 and 4.2 for particular choices of parameter values (e.g., $\Delta t = 10^{-3}$ and 10^{-4} s) with $l' \sim 10^2$–10^3 are therefore expected to characterize the emission also for other choices of parameters with similar values of l'.

4.1. *Low Compactness*

Figure 4 shows spectra obtained for low compactness, $l' \lesssim 3$. Synchrotron self-absorption results in a quasi-thermal spectrum at low energies, below $\varepsilon_{\rm ssa} \approx 100$ eV–1 keV. Between $\varepsilon_{\rm ssa}$ and $\varepsilon_{\rm peak} \approx 10$–100 keV, the spectral index is softer than expected for synchrotron emission only: $\nu F_\nu \propto \nu^\alpha$

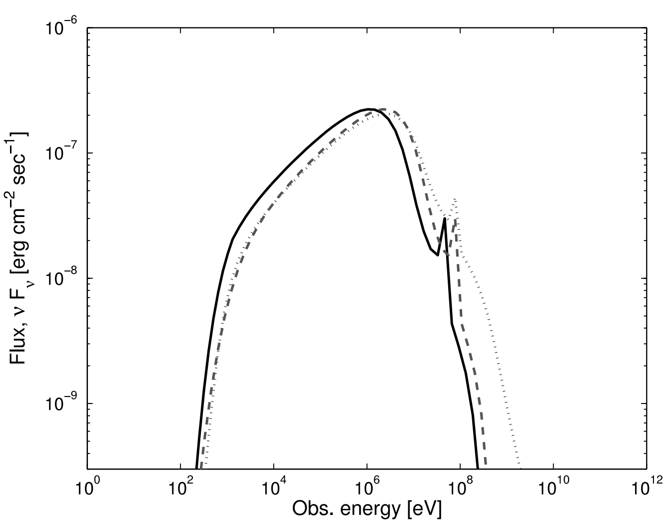

FIG. 3.—Effect of adiabatic expansion on emergent spectra for large compactness ($l' = 250$): *Dotted line*: Spectrum at the end of the dynamical time (before adiabatic expansion); *dashed line*: spectrum after adiabatic expansion; *solid line*: spectrum after correction for energy loss due to plasma bulk motion (see § 3.2). [*See the electronic edition of the Journal for a color version of this figure.*]

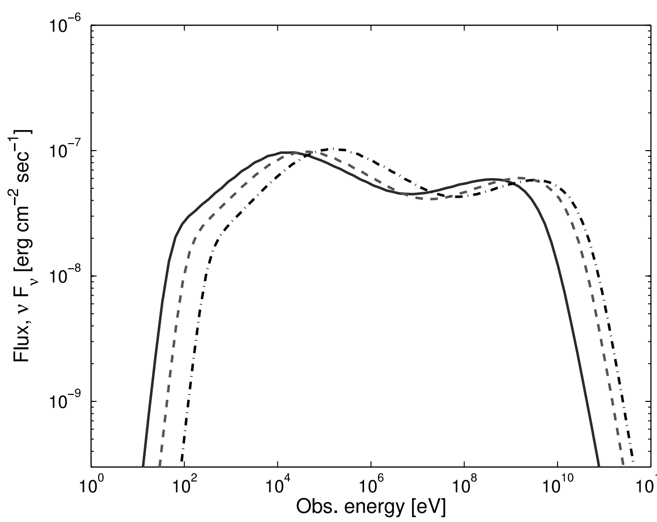

FIG. 4.—Time-averaged spectra obtained for low compactness. Results are shown for $L = 10^{52}$ ergs, $\epsilon_e = \epsilon_B = 10^{-0.5}$, $p = 3$ (all cases) and $\Delta t = 10^{-2}$ s, $\Gamma = 300$ (*solid line*); $\Delta t = 10^{-3}$ s, $\Gamma = 600$ (*dashed line*); and $\Delta t = 10^{-4}$ s, $\Gamma = 1000$ (*dash-dotted line*). The compactness parameter is $l' = 2.5$, 0.8, and 0.6, respectively. Luminosity distance $d_L = 2 \times 10^{28}$ and $z = 1$ were assumed. [*See the electronic edition of the Journal for a color version of this figure.*]

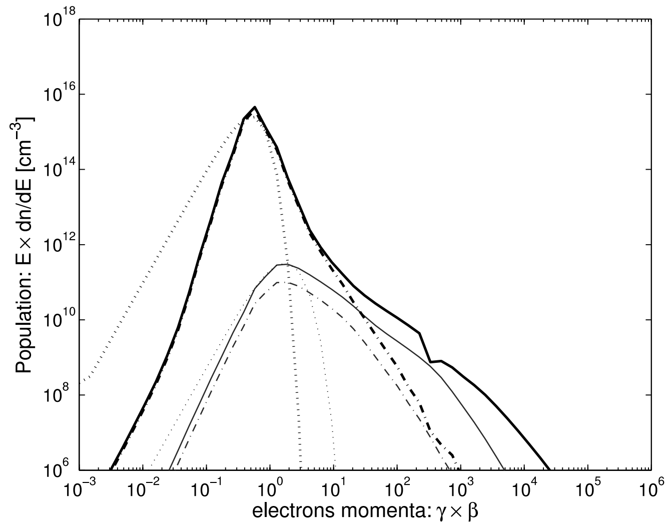

FIG. 5.—Particle distribution at the end of the dynamical time. *Thick solid line*: $\Delta t = 10^{-4}$ s, $p = 3.0$, $\Gamma = 300$, $l' = 250$; *thin solid line*: $\Delta t = 10^{-4}$ s, $p = 3.0$, $\Gamma = 1000$, $l' = 0.6$. All other parameters are the same as in Fig. 4. *Solid lines*: Electron distribution; *dash-dotted lines*: positron distribution. The dotted lines show Maxwellian distributions at temperatures $\theta \equiv kT/m_e c^2 = 0.08$ (*thick line*) and $\theta = 0.5$ (*thin line*). [*See the electronic edition of the Journal for a color version of this figure*.]

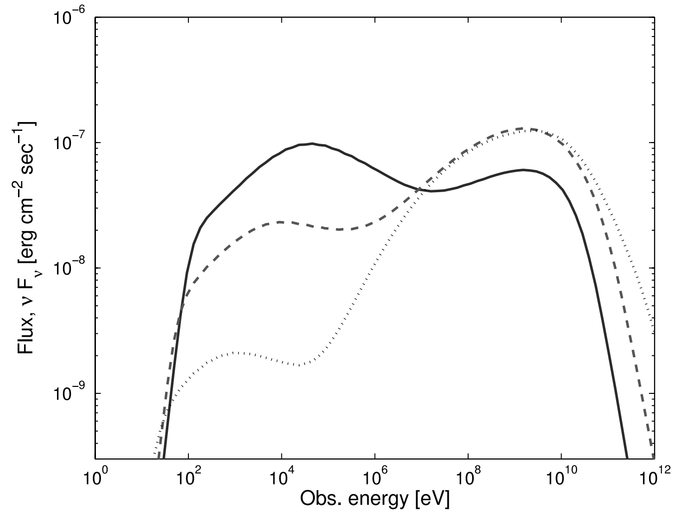

FIG. 7.—Dependence on the fraction of thermal energy carried by magnetic field, ϵ_B, for low compactness. Results are shown for $\Delta t = 10^{-3}$ s, $\Gamma = 600$, $l' = 0.8$, and $\epsilon_B = 0.33$ (*solid line*), 10^{-2} (*dashed line*), and 10^{-4} (*dotted line*). All other parameters are the same as in Fig. 4. The ratio of fluxes at 1 GeV and 0.1 MeV is a good indicator for the ratio $\epsilon_B : \epsilon_e$. [*See the electronic edition of the Journal for a color version of this figure*.]

with $\alpha \approx 0.3$ rather than $\alpha \approx 0.5$. The reason for this deviation is related to the particle population, presented in Figure 5. The self-absorption phenomenon causes particles to accumulate at low-to-intermediate energies, forming a quasi-Maxwellian distribution with temperature $\theta \approx 0.5$. Therefore, above this energy, the electron spectral index is somewhat softer than the spectral index expected without the self-absorption phenomenon ($dn_e/d\varepsilon_e \propto \varepsilon_e^{-2.4}$, instead of $dn_e/d\varepsilon_e \propto \varepsilon_e^{-2}$), resulting in a steeper slope above $\varepsilon_{\rm ssa}$.

Between $\varepsilon_{\rm peak} \approx 10-100$ keV and 10 MeV the spectral slope, $\alpha \approx -0.3$, is harder than expected ($\alpha = -0.5$ for $p = 3.0$) because of significant IC emission. The combined effects of a relatively soft spectrum at low energies and the cooling of particles by both synchrotron emission and Compton scattering lead to the creation of a very soft spectrum ($\alpha \approx 0.1$) near the IC peak at high energies (3–30 GeV). It is therefore concluded that for low compactness, $l' \lesssim 3$, and $\epsilon_B \simeq \epsilon_e$, the spectrum expected at all energy bands between $\sim$100 eV and 30 GeV is flat, with a spectral index that varies in the range $-0.3 \lesssim \alpha \lesssim +0.3$.

The flattening of the spectrum due to both synchrotron and IC scattering decreases the dependence on p. As presented in Figure 6, for $p = 2.0$ the flux rises slowly in all energy bands because of IC scattering, while for $p = 2.5$ it is nearly constant in the 1 keV–1 GeV range.

The dependence of the spectrum on the magnetic field equipartition fraction is shown in Figure 7, which demonstrates that comparison of the fluxes at 1 GeV and 100 keV may allow the determination of the value of ϵ_B.

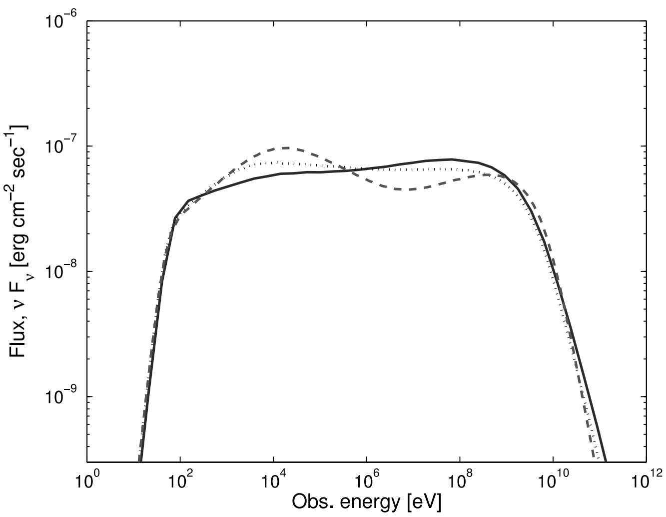

FIG. 6.—Dependence of spectra on the power-law index p of accelerated electrons for low compactness. Results are shown for $\Delta t = 10^{-2}$ s, $\Gamma = 300$, $l' = 2.5$, and $p = 2.0$ (*solid line*), 2.5 (*dotted line*), and 3.0 (*dashed line*). All other parameters are the same as in Fig. 4. Spectra depend only weakly on p. [*See the electronic edition of the Journal for a color version of this figure*.]

4.2. *High Compactness*

Figure 8 presents results for large compactness. When the compactness is large enough, Compton scattering by pairs becomes the dominant emission mechanism. The spectrum cannot be approximated in this case by the commonly used optically thin synchrotron self-Compton model. As demonstrated in Figure 5, electrons and positrons lose their energy much faster than the dynamical timescale, and quasi-Maxwellian distribution with an effective temperature $\theta \simeq 0.05-0.1$ is formed. The energy gain of the low-energy electrons by direct Compton scattering results in a spectrum steeper than Maxwellian at the low-energy end, indicating that a steady state did not develop. As shown in Figure 9, the electron distribution approaches a Maxwellian at the end of the adiabatic expansion. The self-absorption frequency $\varepsilon_{\rm ssa}^{\rm ob} \approx 3-10$ keV *before* the adiabatic expansion (see Fig. 3) is well approximated by equation (10), valid for thermal distribution of electrons.

The ratio of pair to proton number densities at the end of the dynamical time is $f \equiv n_\pm/n_p \simeq 10$ in the calculations shown in Figure 8, in agreement with the analytical approximations of § 2.2. This ratio is determined by the balance between pair production and pair annihilation and leads to

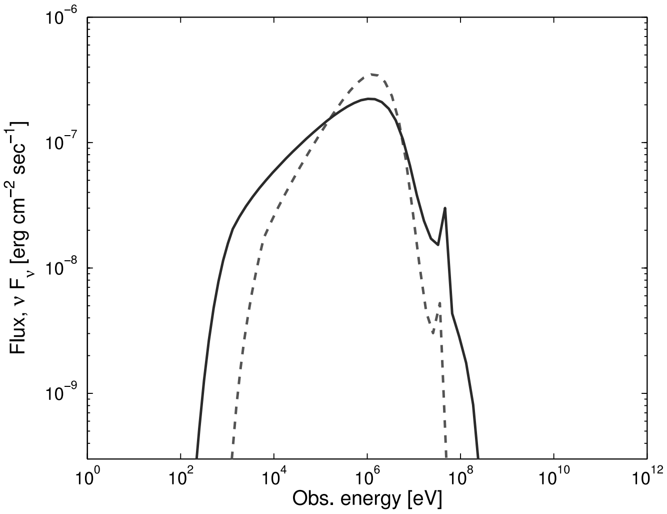

FIG. 8.—Time-averaged spectra obtained for high compactness. Results are shown for $L = 10^{52}$ ergs, $\epsilon_e = \epsilon_B = 10^{-0.5}$, $p = 3$ (all cases) and $\Delta t = 10^{-4}$ s, $\Gamma = 300$ (*solid line*); and $\Delta t = 10^{-5}$ s, $\Gamma = 300$ (*dashed line*). The compactness parameter is $l' = 250$ and 2500, respectively. The scattering optical depth at the end of the dynamical time is 13 and 56, respectively. The peaks observed at ~80 MeV result from pair annihilation. Luminosity distance $d_L = 2 \times 10^{28}$ and $z = 1$ were assumed. [*See the electronic edition of the Journal for a color version of this figure.*]

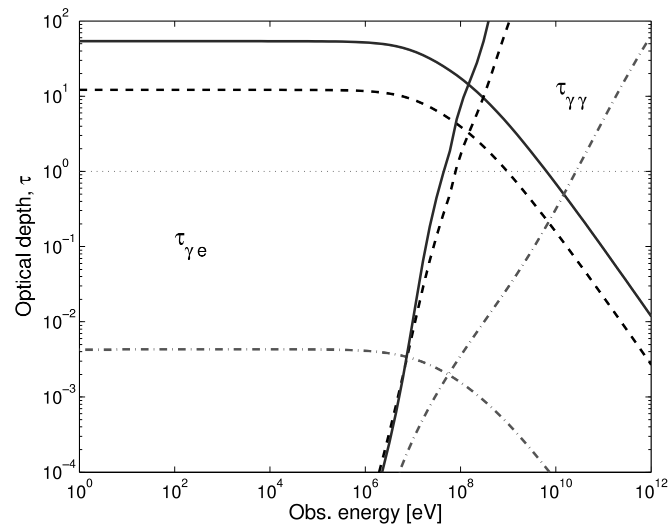

FIG. 10.—Energy-dependent optical depths for pair production and scattering. *Solid lines*: $\Delta t = 10^{-5}$ s, $p = 3.0$, $\Gamma = 300$, and $l' = 2500$; *dashed lines*: $\Delta t = 10^{-4}$ s, $p = 3.0$, $\Gamma = 300$, and $l' = 250$; *dash-dotted lines*: $\Delta t = 10^{-4}$ s, $p = 3.0$, $\Gamma = 1000$, and $l' = 0.6$. All other parameters are the same as in Fig. 4. [*See the electronic edition of the Journal for a color version of this figure.*]

optical depth $\tau_\pm \simeq l'^{1/2}$ (Fig. 10), in accordance with the predictions of § 2.2. Pair annihilation creates the peak at $\Gamma m_e c^2 \sim 10^2 \Gamma_{2.5}$ MeV for large compactness.

An intermediate number of scatterings, $\tau_\pm \lesssim 20$, as is the case for $\Delta t = 10^{-4}$ s (Figs. 3 and 10), leads to moderate value of the Compton y-parameter. If the electron distribution is approximated as a Maxwellian with temperature $\theta \approx 0.1$ (see Fig. 5), the Compton y-parameter, $y \simeq 4\theta\tau \approx 4\theta_{-1}\tau_1$ is not much higher than 1. In this scenario, the number of scatterings is not large enough to create a $\nu F_\nu \propto \nu^1$ spectrum, expected when Comptonization is the dominant emission mechanism (note that the observed spectral indices at 1–10 keV reported by Crider et al. 1997; Frontera et al. 2000 and Preece et al. 2002 are even harder than this value). The resulting spectrum obeys $\nu F_\nu \propto \nu^\alpha$ with $\alpha \approx 0.5$ between $\varepsilon_{\rm ssa} \approx 3-10$ keV and $\varepsilon_{\rm peak} \approx 10$ MeV. For $\Delta t = 10^{-5}$ s, the optical depth is $\tau_\pm \approx 60$ and the Compton y-parameter is higher, $y \approx 25$, resulting in a steeper slope. However, even in this scenario the slope is $\alpha \approx 0.7$ and not the limiting value, $\alpha = 1$.

Since the dominant emission mechanism is Compton scattering by the quasi-thermally distributed particles, the spectrum is independent of most of the physical parameters related to particle acceleration. As is seen in Figure 11, the spectra

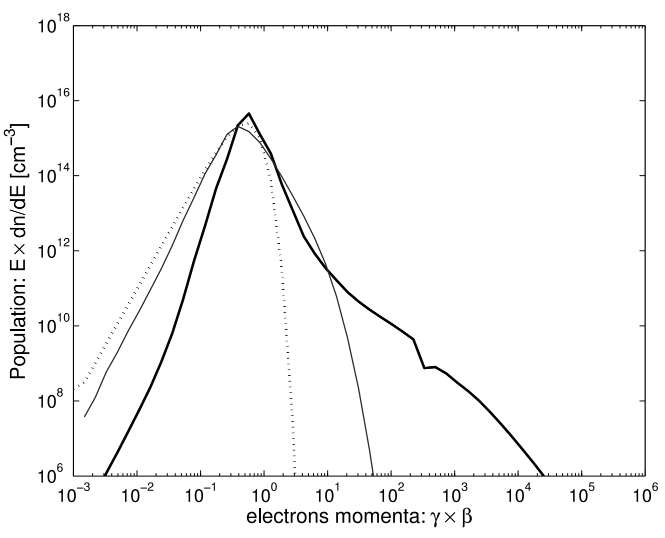

FIG. 9.—Electron energy distribution before and after the adiabatic expansion phase, for $\Delta t = 10^{-4}$ s, $p = 3.0$, $\Gamma = 300$, and $l' = 250$ (and all other parameters the same as in Fig. 4). *Thick line*: Distribution at the end of the dynamical time; *thin line*: distribution at the end of the adiabatic expansion. The dotted line shows a Maxwellian distribution with temperature $\theta \equiv kT/m_e c^2 \approx 0.08$. The particle distribution approaches Maxwellian only at the end of the adiabatic expansion phase. [*See the electronic edition of the Journal for a color version of this figure.*]

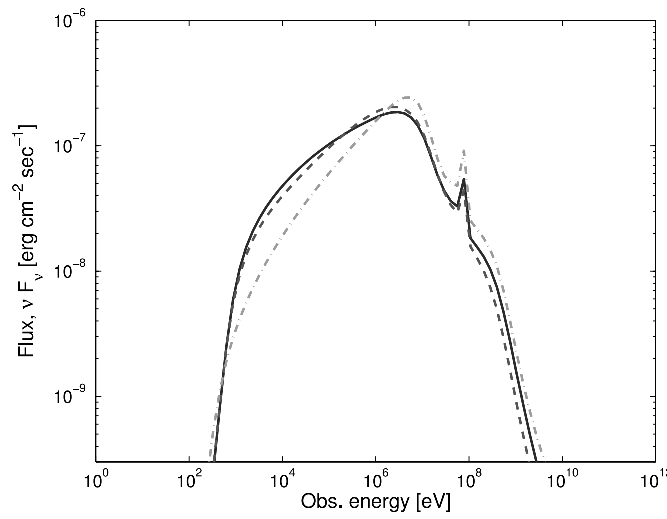

FIG. 11.—Dependence of spectra on the power-law index p of accelerated electrons and on the fraction of thermal energy carried by magnetic field, ϵ_B, for high compactness. Results shown for $\Delta t = 10^{-4}$ s, $\Gamma = 300$, $l' = 250$ and $p = 2.0$, $\epsilon_B = 0.33$ (*solid line*); $p = 3.0$, $\epsilon_B = 0.33$ (*dashed line*); and $p = 2.0$, $\epsilon_B = 0.01$ (*dash-dotted line*). All other parameters are the same as in Fig. 4. Spectra depend only weakly on p and ϵ_B. [*See the electronic edition of the Journal for a color version of this figure.*]

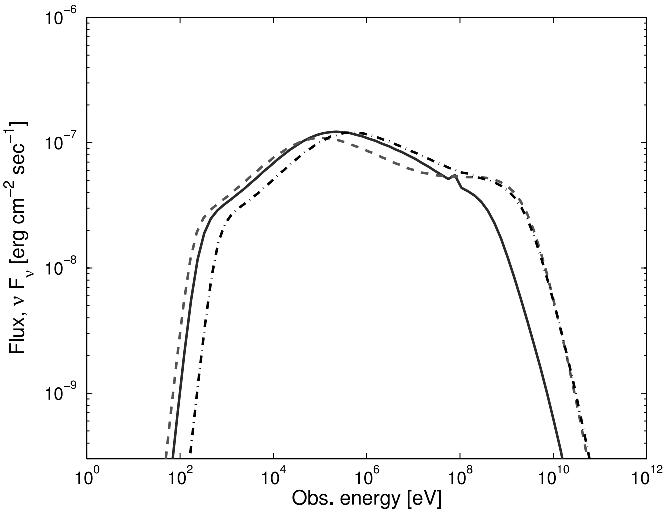

FIG. 12.—Time-averaged flux obtained for intermediate compactness. *Solid line*: $\Delta t = 10^{-3}$ s, $\Gamma = 300$; *dashed line*: $\Delta t = 10^{-3}$ s, $\Gamma = 400$; *dash-dotted line*: $\Delta t = 10^{-4}$ s, $\Gamma = 600$. All the other fireball model parameters are the same as in Fig. 4. The compactness parameter is $l' = 25$, 6, and 8, respectively. [*See the electronic edition of the Journal for a color version of this figure*.]

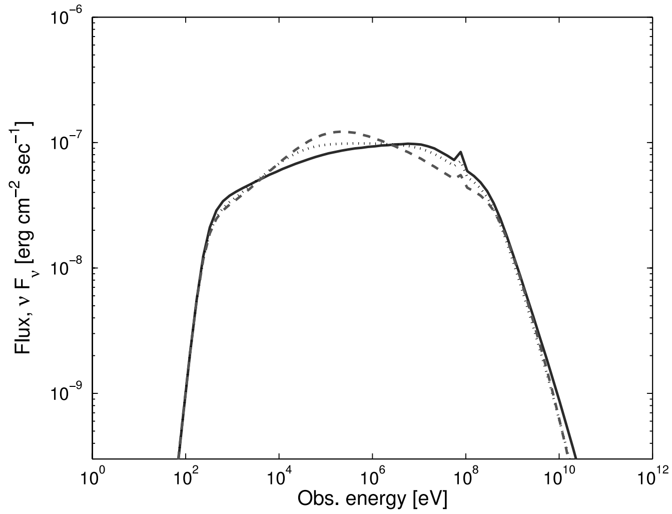

FIG. 13.—Dependence of spectra on the power-law index p of accelerated electrons for intermediate compactness. Results shown for $\Delta t = 10^{-3}$ s, $\Gamma = 300$, $l' = 25$, and $p = 2.0$ (*solid line*), 2.5 (*dotted line*), and 3.0 (*dashed line*). All other parameters are the same as in Fig. 4. [*See the electronic edition of the Journal for a color version of this figure*.]

do not depend on the power-law index of the accelerated electrons. The dependence on ϵ_B is weak; a smaller ϵ_B gives a steeper slope between 1 keV–10 MeV.

If l' is large, the flux is rising up to 1 MeV, regardless of the value of p. Therefore, observing a decrease in the flux between 30 keV and 1 MeV indicates both that $p > 2$ and that $l' \lesssim 3$.

4.3. *Intermediate Compactness*

For l' in the range of a few to a few tens, synchrotron emission and Compton scattering equally contribute to the observed radiation. Here too, the spectrum cannot be approximated by simple analytic formulation. Figure 12 shows several examples of spectra obtained for moderate l'.

Even though a significant number of pairs are created, $f \sim 10$ for the three scenarios presented in Figure 12, the optical depth for scattering is approximately 1, and the self-absorption frequency is $\varepsilon_{\rm ssa} \sim 1$ keV. Although the number of scatterings is not large, it is sufficient for increasing the energy at which the spectrum peaks by about a factor of 3 above the synchrotron model prediction, leading to $\varepsilon_{\rm peak} \sim 500$ keV for ϵ_e and ϵ_B near equipartition. Lower ϵ_B leads to higher $\varepsilon_{\rm peak}$, while lower ϵ_e leads to lower $\varepsilon_{\rm peak}$.

The spectral slope in the 1 keV–1 MeV range is soft, $\alpha \simeq 0.3$, instead of the expected value of $\alpha \approx 0.5$, similar to the spectra produced for small l', for similar reasons. Figure 13 shows that the exact power law of the accelerated electrons has only a minor influence on the observed spectra.

A significant flux is expected up to $\gtrsim$1 GeV. Unlike in the scenario of very small l', the flux decreases above $\varepsilon_{\rm peak}$, and no second peak due to IC scattering from high-energy electrons is formed. This phenomenon is due to pair production, which cuts off the flux above the energies at which such a peak would form, $\sim$1 GeV. Therefore, the main characteristics of spectra produced by intermediate values of l' are a moderate increase in the flux in the 1 keV to 1 MeV energy bands, a moderate decrease in the flux in the 1 MeV to 1 GeV band, and a sharp cutoff above this energy.

5. QUASI-THERMAL COMPTONIZATION

We consider in this section the quasi-thermal Comptonization scenario proposed by Ghisellini & Celotti (1999). This model is different from the one considered in the previous section in that (1) we assume that the kinetic energy dissipated in two-shell collision is continuously distributed among all shell electrons, rather than being deposited at any given time into a small fraction of the shell electrons that pass through the shock wave, and (2) we assume that energy is equally distributed among electrons, rather than following a power-law distribution. In this case, no highly relativistic electrons are produced, and Comptonization is the main mechanism responsible for emission above a few keV: synchrotron emission is self-absorbed up to frequency ν_t, providing the seed photons for Comptonization to create a $\nu F_\nu \propto \nu^1$ spectrum up to $\varepsilon_{\rm peak}$. We derive here the constraints on the peak flux energy $\varepsilon_{\rm peak}$ in this scenario, both analytically and numerically.

Figure 14 presents numerical results obtained for this scenario. The calculations were carried out using a modified version of the numerical model, in which electrons and positrons are forced to follow a Maxwellian distribution, $n(\gamma)\, d\gamma \propto \beta\gamma^2 e^{-\gamma/\theta}\, d\gamma$. The temperature $\theta(t)$ is determined self-consistently by the balance of energy injection and energy loss. The results are shown for two representative cases in Figure 14. In both cases, electrons and positrons reach a mildly relativistic temperature, $\theta \sim 0.3$, and the spectrum peaks at $\varepsilon_{\rm peak} \approx 30$ MeV. The spectral slope below $\varepsilon_{\rm peak}$ is $\alpha \approx 0.5$ ($\nu F_\nu \propto \nu^\alpha$) for $\Delta t = 10^{-3}$ s, where $\tau_\pm \sim 2$, and $\alpha \approx 1$ for $\Delta t = 10^{-4}$ s, where $\tau_\pm \sim 10$. In the former case, the scattering optical depth, $\tau_\pm \sim 2$, is not large enough to produce the $\alpha \simeq 1$ spectrum expected for $\tau_\pm \gg 1$. We show below, using analytic analysis, that $\varepsilon_{\rm peak} \gtrsim 30$ MeV is a generic result of the thermal Comptonization scenario.

In an expanding plasma characterized by width ΔR, the available time for scattering is $\Delta R/c$ and the time between scattering is $\langle l \rangle/c$, where $\langle l \rangle$ is the mean free path. Therefore, the number of scatterings, $N \approx \Delta R/\langle l \rangle$, is proportional to τ, and the Compton y-parameter is given by

$$y = 4\theta\tau = 4\theta\Delta R\sigma_{\rm T} n_p f = 4\theta\Gamma c\Delta t\sigma_{\rm T} n_p f. \qquad (17)$$

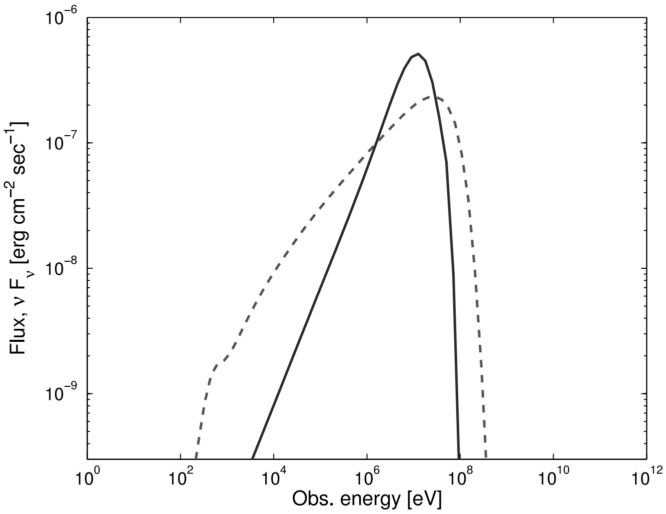

FIG. 14.—Time-averaged flux for the quasi-thermal Comptonization scenario. Fireball model parameters assumed are $L = 10^{52}$ ergs s^{-1}, $\Gamma = 300$, $\epsilon_e = \epsilon_B = 0.33$, and $\Delta t = 10^{-3}$ s (*dashed line*) or $\Delta t = 10^{-4}$ s (*solid line*). [*See the electronic edition of the Journal for a color version of this figure.*]

The synchrotron spectrum is well approximated by blackbody radiation up to frequency ν_t, given in equation (9). Thus, the observed luminosity is given by

$$\frac{L}{\Gamma^2} = e^y L_{\rm sync} = e^y \frac{8\pi}{3} m_e r_i^2 \theta \nu_t^3, \qquad (18)$$

and the observed emission peaks at

$$\varepsilon_{\rm peak}^{\rm ob} = e^y h\nu_t \Gamma. \qquad (19)$$

In the following calculation, we assume that $e^y h\nu_t\Gamma$ is not larger than the saturation value of $\varepsilon_{\rm peak}^{\rm ob}$, $4\theta\Gamma m_e c^2$. If this is not the case, for $\Gamma = 10^{2.5}$, $\theta \approx 10^{-3}$ is needed in order to obtain $\varepsilon_{\rm peak}^{\rm ob} \approx 1$ MeV. Since $y >$ a few is required, this value of θ implies a very large optical depth, $\tau \approx 10^3$. Such a large value is not obtained for parameter values relevant for GRB fireballs and would lead to strong suppression of emitted radiation.

Assuming that $\varepsilon_{\rm peak}^{\rm ob}$ is given by equation (19), since $\theta \leq 1$, in order to get $y >$ a few photons have to undergo a minimum number of scatterings, i.e., $\tau \gtrsim$ a few. For a minimum value of $\tau = 10^{0.5}\tau_{0.5}$, with $\tau = \Delta R \sigma_{\rm T} n_p f$, f is given by

$$f = 4L_{52}^{-1}\Delta t_{-4}\tau_{0.5}. \qquad (20)$$

Eliminating e^y from equations (18) and (19) using equation (9), θ is given by

$$\theta = 1.7 f^{-1/9} L_{52}^{-2/30} \epsilon_{B,-0.5}^{-0.3} \left(\varepsilon_{\rm peak,1\,MeV}^{\rm ob}\right)^{-1/3} \Gamma_{2.5}^{5/9}, \qquad (21)$$

and the Compton y-parameter (eq. [17]) becomes

$$y = 4\theta\tau = 5.5 f^{8/9} L_{52}^{14/15} \epsilon_{B,-0.5}^{-0.3} \Gamma_{2.5}^{-40/9} \Delta t_{-4}^{-1} \left(\varepsilon_{\rm peak,1\,MeV}^{\rm ob}\right)^{-1/3}. \qquad (22)$$

Using the values obtained for ν_t (eq. [9]) and θ (eq. [21]) in equation (19), we obtain

$$e^y = \frac{\varepsilon_{\rm peak}}{h\nu_t\Gamma} = 135 f^{-1/18} L_{52}^{-8/15} \epsilon_{B,-0.5}^{-0.15} \left(\varepsilon_{\rm peak,1\,MeV}^{\rm ob}\right)^{4/3} \Gamma_{2.5}^{16/9} \Delta t_{-4}. \qquad (23)$$

The very weak dependence of the right-hand side on f allows us to eliminate it. Taking $f^{1/18} \approx 1$, one can take the log of both sides and use equation (22) to express f,

$$f \approx 0.55 L_{52}^{-21/20} \epsilon_{B,-0.5}^{27/80} \Gamma_{2.5}^{5} \Delta t_{-4}^{9/8} \left(\varepsilon_{\rm peak,1\,MeV}^{\rm ob}\right)^{3/8}. \qquad (24)$$

Equation (20) then gives

$$\varepsilon_{\rm peak}^{\rm ob} = 200(1+z)^{-1} L_{52}^{2/15} \epsilon_{B,-0.5}^{-9/10} \Delta t_{-4}^{-1/3} \tau_{0.5}^{8/3} \text{ MeV}. \qquad (25)$$

Since ϵ_B already assumes its maximum value, the only way to meet the observed peak flux $\varepsilon_{\rm peak}^{\rm ob} \approx 1$ MeV in this scenario is by assuming a significantly lower value of total luminosity or longer variability time Δt, both inconsistent with the parameter space region for high compactness, as well as with the observations. Note that the observed peak would be obtained at an energy somewhat lower than that given by equation (25) because of pair production, which leads to a cutoff at $\Gamma m_e c^2 = 150\Gamma_{2.5}$ MeV.

The above analysis shows that in the "slow heating scenario" the flux cannot peak below a few hundred MeV. This general result is not changed by the adiabatic expansion, during which the optical depth decreases according to $\tau(t) = \tau_0[\Delta R/(\Delta R + vt)]^2$, where τ_0 is the optical depth before the expansion and $v \approx c/\sqrt{3}$ is the expansion velocity. The total number of scatterings increases during the adiabatic expansion by a factor of $(1+\sqrt{3}) \approx 3$ compared to the number of scatterings at the dynamical time. This factor enters equations (20) and (24) with nearly the same power (1 in eq. [20], 9/8 in eq. [24]), leaving the final conclusion unchanged.

6. SUMMARY AND DISCUSSION

Within the fireball model framework, synchrotron emission peaking at $\sim$1 MeV may be obtained with small compactness, $l' \sim 1$, only for very short variability time, $\Delta t \leq 10^{-4.5}$ s, and large Γ, $\Gamma \geq 10^3$ (see eqs. [12] and [11], in § 2.2). For the longer variability time commonly assumed in modeling GRBs, $\Delta t \sim 1$ to 10 ms (e.g., Piran 2000; Mészáros 2002; Waxman 2003), $l' \sim 10^2$–10^3 is obtained for the parameter range in which synchrotron emission peaks at $\sim$1 MeV (for smaller compactness, spectra peak at lower, X-ray, energy). This result has two main consequences. First, observed GRB spectra are expected to be significantly modified by the presence of pairs. Second, peak energy $\gg$1 MeV cannot be obtained for $L \sim 10^{52}$ ergs s^{-1}, since it would imply that $l' \gg 10^3$ (see eqs. [12], [16], and [15]), in which case most of the radiation will not escape because of large optical depth to Thomson scattering by pairs. These conclusions are consistent with the conclusions of Guetta et al. (2001) and may provide an explanation for the lack of bursts with peak energy $\gg$1 MeV.

It should be noted at this point that GRB observations do not allow, in most cases, the identification of variability on a

$\sim$1 ms timescale. Rapid variability, on a $\sim$1 ms timescale, has been observed in some bursts (Bhat et al. 1992; Fishman et al. 1994), and most bursts show variability on the shortest resolved timescale, $\sim$10 ms (Woods & Loeb 1995; Walker et al. 2000). It should be kept in mind, however, that variability on much shorter timescales would not have been possible to resolve experimentally and therefore cannot be ruled out.

We have demonstrated in § 2.2 that for l' in the range of 10^2–10^3 the characteristics of emitted radiation are determined mainly by l', with weak dependence on the values of other parameters (see, e.g., eq. [15]). The peak of the specific luminosity is expected to be close to $\sim$1 MeV, $\sim 1\left(L_{52}/\Delta_{t,-3}\right)^{1/5}$ $(l'/100)^{-1}$ MeV (eq. [15]), and the spectrum is expected to differ significantly from an optically thin synchrotron spectrum.

These conclusions are consistent with the results of our detailed numerical calculations. We have presented numerical results of calculations of prompt GRB spectra within the fireball model framework, using a time-dependent numerical code that describes cyclo-synchrotron emission and absorption, inverse and direct Compton scattering, and $e^{\pm}$ pair production and annihilation. We have shown that the spectral shape depends mainly on the compactness parameter, which is most sensitive to the fireball Lorentz factor Γ, $l' \propto \Gamma^{-5}$. For large compactness (small Γ), $l' > 100$, the spectra peak at $\sim$1 MeV, show steep slopes at lower energy, $\varepsilon^2 dN/d\varepsilon \propto \varepsilon^{\alpha}$ with $0.5 < \alpha < 1$, and show a sharp cutoff at $\sim$10 MeV (see Fig. 8). The spectra depend only weakly in this regime on the power-law index p of accelerated electrons and on the magnetic field energy fraction ϵ_B (see Fig. 11). For small-to-moderate compactness (large Γ), $l' \lesssim 10$, spectra extend to $\gtrsim$10 GeV (see Figs. 4 and 12). The spectrum at lower energy depends only weakly on p (see Fig. 6), but strongly on ϵ_B (see Fig. 7). For a magnetic field close to equipartition, spectra peak at $\sim$0.1 MeV for $l' \sim 10$ and extend to higher energy with spectral index $\alpha = 10^{0\pm0.5}$.

Since moderate-to-large compactness is required for a synchrotron peak at $\sim$1 MeV, the effects of pair-production and direct Compton and IC scattering by pairs are predicted to be large for observed GRBs. In this case, simple analytic approximations of synchrotron self-Compton emission do not provide an accurate description of the emergent spectra. In particular, Compton scattering by the pairs, which are accumulated at intermediate energy $\theta \equiv \varepsilon/m_e c^2 \approx 0.1$ (see Fig. 9), results in a steep slope, $0.5 \le \alpha \le 1$, in the 1 keV–1 MeV band. A still steeper slope, $\alpha \approx 3$, is obtained at lower energies, below the self-absorption frequency determined by the quasi-thermal pair distribution, $\varepsilon_{\rm ssa}^{\rm ob} \approx 10^{0.5\pm0.5}$ keV (see eq. [10]). These steep slopes may account for the steep slopes observed at early times in some GRBs (see Frontera et al. 2000; Preece et al. 2002; Ghirlanda et al. 2003).

The spectra presented in this paper (§ 4) describe the emission resulting from a single collision within the expanding fireball wind, for various choices of model parameters (e.g., L, Δt, Γ). Observed spectra are expected to be combinations of spectra produced by many single-shell collisions, each characterized by different parameters. This is due to the fact that at any given time a distant observer is expected to receive radiation from many collisions taking place at various locations within the wind. Moreover, observed spectra are inferred from measurements in which the signal is integrated over time intervals longer than that expected for the duration of a single collision. A detailed comparison with observations requires a detailed model describing the distribution of single-shell collision parameters within the fireball wind (see, e.g., Daigne & Mochkovitch 1998; Panaitescu et al. 1999; Guetta et al. 2001). The construction and investigation of such models are beyond the scope of this manuscript.

We have shown (§ 5, Fig. 14) that the quasi-thermal Comptonization scenario (e.g., Ghisellini & Celotti 1999), in which kinetic energy dissipated in shocks is continuously distributed roughly equally among all electrons, leads to high peak energy, $\gtrsim$30 MeV. This scenario may not account, therefore, for observed GRB spectra.

Clearly, the most stringent constraints on l', and hence on Γ, will be provided by measurements of the spectra at high energy $\gtrsim$0.1 GeV. The fluxes predicted by the model are detectable by *GLAST*.[2] For large compactness, where emission is strongly suppressed above 0.1 GeV, the model predicts a steep spectrum at low energy, which is weakly dependent on other model parameters (Fig. 11). For small compactness, where strong emission is expected above 10 MeV, the low-energy spectrum depends mainly on ϵ_B (Fig. 7). Comparison of the flux at $\sim$1 GeV and $\sim$100 keV (available, e.g., with *Swift*[3]) may therefore allow the determination of the fireball magnetic field strength. Stringent constraints on p, the spectral index of the energy distribution of accelerated electrons, will be difficult to obtain, because of the weak dependence of spectra on this parameter.

This work was supported in part by a Minerva grant and by an ISF grant.

[2] See http://www-glast.stanford.edu.
[3] See http://www.swift.psu.edu.

REFERENCES

Bekefi, G. 1966, Radiation Processes in Plasmas (New York: Wiley)
Bhat, P. N., et al. 1992, Nature, 359, 217
Bötcher, M., & Schlickeiser, R. 1997, A&A, 325, 866
Crider, A., et al. 1997, ApJ, 479, L39
Daigne, F., & Mochkovitch, R. 1998, MNRAS, 296, 275
Fishman, G. J., et al. 1994, ApJS, 92, 229
Frontera, F., et al. 2000, ApJS, 127, 59
Ghirlanda, G., Celotti, A., & Ghisellini, G. 2003, A&A, 406, 879
Ghisellini, G., & Celotti, A. 1999, ApJ, 511, L93
Ghisellini, G., Lazzati, D., Celotti, A., & Rees, M. J. 2000, MNRAS, 316, L45
Ginzburg, V. L., & Syrovatskii, S. I. 1969, ARA&A, 7, 375
Guetta, D., Spada, M., & Waxman, E. 2001, ApJ, 557, 399
Jones, F. C. 1968, Phys. Rev., 167, 1159
Lazzati, D., Ghisellini, G., Celotti, A., & Rees, M. J. 2000, ApJ, 529, L17
Lightman, A. P. 1982, ApJ, 253, 842
Lightman, A. P., & Zdziarski, A. A. 1987, ApJ, 319, 643
Mahadevan, R., Narayan, R., & Yi, I. 1996, ApJ, 465, 327
Mészáros, P. 2002, ARA&A, 40, 137
Mészáros, P., Ramirez-Ruiz, E., Rees, M. J., & Zhang, B. 2002, ApJ, 578, 812
Mészáros, P., & Rees, M. J. 2000, ApJ, 530, 292
Panaitescu, A., Spada, M., & Mészáros, P. 1999, ApJ, 522, L105
Pilla, R. P., & Loeb, A. 1998, ApJ, 494, L167
Piran, T. 2000, Phys. Rep., 333, 529
Preece, R. D., et al. 2002, ApJ, 581, 1248
Rybicki, G. B., & Lightman, A. P. 1979, Radiative Processes in Astrophysics (New York: Wiley)
Sunyaev, R. A., & Titarchuk, L. G. 1980, A&A, 86, 121

Svensson, R. 1982a, ApJ, 258, 321
———. 1982b, ApJ, 258, 335
———. 1984, MNRAS, 209, 175
———. 1987, MNRAS, 227, 403
Walker, K. C., Schaefer, B. E., & Fenimore, E. E. 2000, ApJ, 537, 264
Waxman, E. 2003, in Supernovae and Gamma-Ray Bursters, ed. K. Weiler (Berlin: Springer), 393
Woods, E., & Loeb, A. 1995, ApJ, 453, 583
Zhang, B., & Mészáros, P. 2002, ApJ, 581, 1236